Prediction of Grain Structures in Various Solidification Processes

M. RAPPAZ, Ch.-A. GANDIN, J.-L. DESBIOLLES, and Ph. THÉVOZ

Grain structure formation during solidification can be simulated *via* the use of stochastic models providing the physical mechanisms of nucleation and dendrite growth are accounted for. With this goal in mind, a physically based cellular automaton (CA) model has been coupled with finite element (FE) heat flow computations and implemented into the code *3-MOS*. The CA enmeshment of the solidifying domain with small square cells is first generated automatically from the FE mesh. Within each time-step, the variation of enthalpy at each node of the FE mesh is calculated using an implicit scheme and a Newton-type linearization method. After interpolation of the explicit temperature and of the enthalpy variation at the cell location, the nucleation and growth of grains are simulated using the CA algorithm. This algorithm accounts for the heterogeneous nucleation in the bulk and at the surface of the ingot, for the growth and preferential growth directions of the dendrites, and for microsegregation. The variations of volume fraction of solid at the cell location are then summed up at the FE nodes in order to find the new temperatures. This CAFE model, which allows the prediction and the visualization of grain structures during and after solidification, is applied to various solidification processes: the investment casting of turbine blades, the continuous casting of rods, and the laser remelting or welding of plates. Because the CAFE model is yet two-dimensional (2-D), the simulation results are compared in a qualitative way with experimental findings.

I. INTRODUCTION

THE grain structure of as-cast components is one of the important features that a metallurgist has to control. As an example, Figure 1 shows the grain structure of a gas turbine blade which has been solidified under directional heat flow conditions. This nickel-base superalloy starts to solidify at the contact with the copper chill under the form of very fine grains (bottom of the blade). From this "outer-equiaxed zone,"[1,2] the grains which have one of their ⟨100⟩ crystallographic orientations best aligned with the heat flow direction (vertical direction in this case) grow preferentially at the expense of less favorably oriented grains. This mechanism of grain selection is due to the ⟨100⟩ preferential growth of dendrites which compose the grains.[1,2] Accordingly, as the columnar grains grow upward, their density in a transverse section decreases. This grain selection mechanism, which has been known for several decades, is currently used in industry to produce single-crystal turbine blades;[3,7] in this case, a specially designed narrow channel inserted between the chill surface and the bottom of the blade allows only one grain to emerge at the top of this "selector." Once the thermal gradient in the remaining liquid becomes small, equiaxed grains can nucleate and grow at the expense of columnar grains, thus leading to the so-called "columnar-to-equiaxed" transition (CET). Such a transition is clearly visible in Figure 1.

The formation and competition of grains during solidification can be studied using different techniques. Metallographic inspection of cast parts such as the one shown in Figure 1 is certainly instructive but does not bring much insight into the mechanisms that lead to such structures. *In situ* microscopy observation of the solidification of transparent organic alloys without doubt has been a major source of information.[4,5,6] With the advent of powerful computers and sophisticated numerical techniques, physical models which integrate nucleation and growth mechanisms have been developed for the simulation of grain structure formation. At first, analytical models similar to the well-known Avrami transformation law were developed for equiaxed grain structures. These so-called *deterministic* models, which have been reviewed in Reference 8, suffer from several limitations: they are based on average entities, they do not provide any view of the microstructure, they do not consider preferential growth directions of dendrites and thus cannot predict grain selection mechanisms, they can hardly account for columnar growth and thus for the CET, the impingement has to be modeled through simplified laws, *etc.*

Many of these drawbacks have been removed with the use of *stochastic* models. The first approach initiated by Brown and Spittle[9,10] was based upon a Monte Carlo (MC) method similar to that previously described by Anderson *et al.*[11] for the prediction of grain growth in solids. Zhu and Smith slightly modified this technique[12] and implemented it in a finite difference (FD) calculation of heat flux.[13] Although the MC method has proved to be successful in producing grain structures which resemble those encountered in real castings, it lacks the physical mechanisms associated with dendritic or eutectic growth.[14] In particular, it does not account for the growth kinetics of dendrite tips (or eutectic front) or the preferential growth directions of dendrites.[1,2] For those reasons, physically based stochastic

M. RAPPAZ, Professor, Ch.-A. GANDIN, Postdoctoral Fellow, and J.-L. DESBIOLLES, Staff Member, are with the Laboratoire de Métallurgie Physique, Département des Matériaux, Ecole Polytechnique Fédérale de Lausanne, CH-1015 Lausanne, Switzerland. Ph. THÉVOZ, Executive Director, is with Calcom SA, PSE, CH-1015 Lausanne, Switzerland.

This article is based on a presentation made at the "Analysis and Modeling of Solidification" symposium as part of the 1994 Fall meeting of TMS in Rosemont, Illinois, October 2–6, 1994, under the auspices of the TMS Solidification Committee.

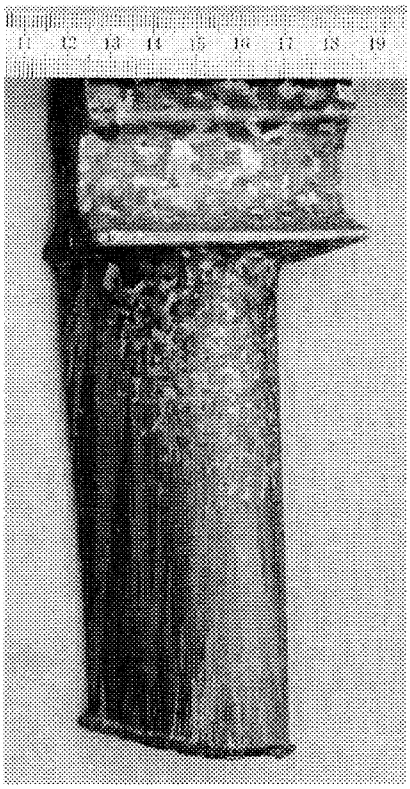

Fig. 1—Columnar and equiaxed grain structures in a nickel-base turbine blade which has been cast over a copper chill plate.

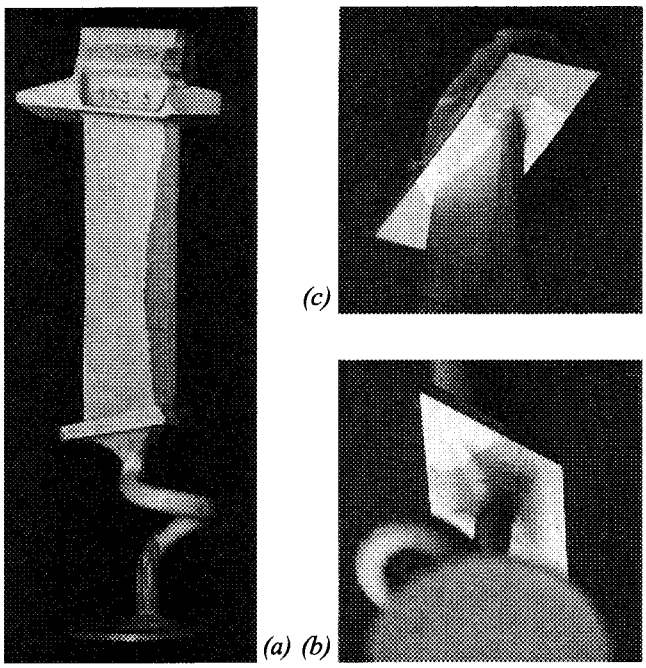

Fig. 2—(*a*) Grain structure in a CMSX6 turbine blade and enlargements of the (*b*) head and (*c*) foot of the blade illustrating the formation of stray crystals. The casting conditions have been chosen on purpose so as to produce stray crystals in the platforms. Height of the cast part shown in (a): 125 mm.

models were developed over the past 4 years for the simulation of eutectic[15,16,17] and dendritic[18–22] grain structure formation under various solidification conditions.

The modeling of dendritic solidification using cellular automaton (CA) was first undertaken for small specimens of uniform temperature in two[18] and three dimensions.[19,20,21] It was shown that the experimental observations made on real castings could be reproduced qualitatively with the two-dimensional (2-D) model (*e.g.*, influence of cooling rate, of alloy concentration, and of inoculation conditions), but that a quantitative comparison with the actual microstructures required a three-dimensional (3-D) description. The predictions of the competition among columnar grains and of the CET were in good agreement with experiment. More recently, the simultaneous evolutions of the density and crystallographic texture of grains belonging to the columnar zone of investment cast superalloys were characterized using an automatic electron backscattered diffraction pattern technique.[21] These evolutions were compared favorably with those calculated using the 3-D CA model, even though the thermal gradient in the specimen was large. Finally, a new 2-D CA algorithm has been developed and coupled with finite element (FE) heat flux calculations in order to handle nonuniform situations.[22] This coupling has been fully integrated within a commercial FE software, *3-MOS*.[23] This so-called CAFE model has been applied to the dendritic growth of organic alloys and to the CET of directionally solidified aluminum alloys.

In the present article, the CAFE model of dendritic solidification is first briefly summarized. It is then applied to several solidification processes, namely, investment casting, continuous casting, and laser remelting or welding. The application of another CA algorithm to the case of welding has already been proposed by Dress *et al.*,[24] but again, the physics of dendritic growth is not taken into account in this model. Although the present comparison with experimental observations is still qualitative, mainly due to the restriction to two dimensions, the present applications clearly demonstrate the potential and versatility of the CAFE approach, as well as the need to extend this method to three dimensions.

II. EXPERIMENTAL OBSERVATIONS

The macrostructure of a turbine blade with its grain selector is shown in Figure 2(a). The CMSX6 superalloy was cast into a preheated mold using the SMCT process,[7] but the experimental conditions used in the present experiment were purposely not optimized in order to illustrate some of the defects that can be encountered in the production of single crystal turbine blades. As can be seen, the airfoil consists of two grains which are revealed after etching by different gray levels. One grain was selected by the pigtail selector, whereas the second one was nucleated near the head of the blade* (Figure 2(b)). These two grains, whose

*Because the blade is cast upside down, the head of the blade corresponds to the platform just above the grain selector.

⟨100⟩ crystallographic orientations were close to the axis of the blade, managed to grow along the whole length of the airfoil. Other stray crystals can also be seen in the upper platform (*i.e.*, foot of the blade shown in Figure 2(c)). The phenomenon of stray crystal formation is particularly critical at section enlargements of the mold, because the den-

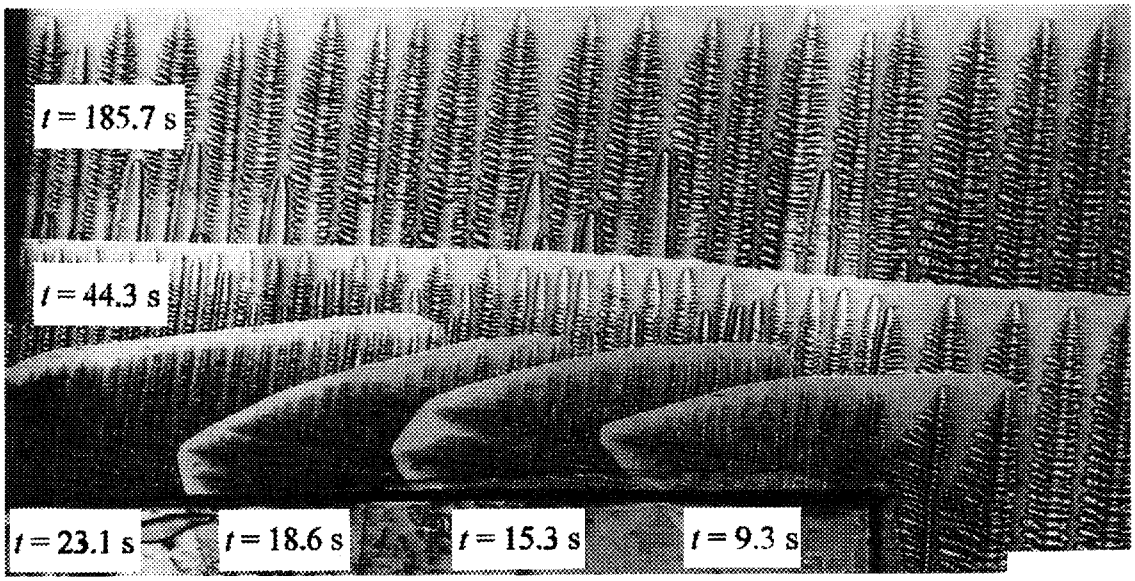

Fig. 3—Development of the dendritic network in a succinonitrile-acetone alloy directionally solidified within two glass plates after passing a re-entrant corner.[25] Six various stages of the dendritic growth recorded using a video camera are superimposed in this picture. The lateral extension of the cell after the re-entrant corner is equal to 4 mm.

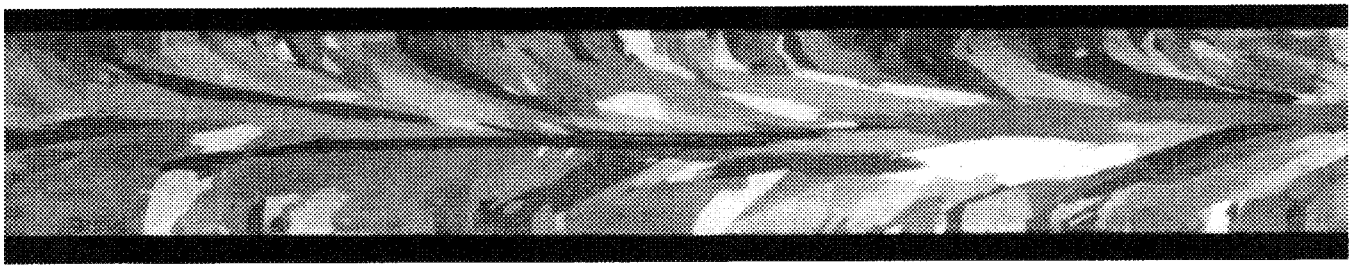

Fig. 4—Grain structure in the longitudinal section of a low-alloyed copper rod (diameter: 20 mm) produced by continuous casting.

dritic network coming from the center has to fill the open space of liquid after passing a re-entrant corner.

The extension of the dendrite arms near such a re-entrant corner and the formation of new trunks from tertiary arms are illustrated in Figure 3 for a succinonitrile-acetone alloy.[25] This alloy was directionally solidified at constant pulling speed between two thin glass plates using a fixed thermal gradient. A plastic insert was employed, above which the liquid zone suddenly widened, in order to simulate the situation of the platforms of investment casting seen in Figure 2. Time-lapse photography showed the evolution of the dendritic structure as solidification proceeded from the narrow to the wide section. Since the liquidus isotherm is almost horizontal, the secondary dendrite arm at the level of the corner becomes more undercooled than the primary dendrite tips. Therefore, it grows much faster in the horizontal direction. Some of the tertiary arms initiated by this secondary branch become new dendrite trunks, which then catch up with the stationary isotherms. Because the non-steady-state undercooling at the tip of the secondary arm is larger than the undercooling of the primary dendrite tips growing under steady-state conditions, the probability of nucleating a stray crystal after the re-entrant corner is increased, as already seen in Figures 2(b) and (c).

Figure 4 illustrates the formation of grains in the longitudinal section of a continuously cast low-alloy copper rod. As can be seen, the grains nucleate mainly at the surface of the rods in contact with the oscillating mold. These grains turn to the right, opposite to the withdrawal direction, as the orientation of the thermal gradient gradually changes from a radial direction near the surface of the rod to a longitudinal direction near the center. Along the centerline of this specimen, the grains are almost parallel to the rod axis and are not connected to the lateral surface. They could have originated from columnar grains formed above or below the section plane or they could have nucleated in the bulk of the liquid.

Similar grain structures can be seen in the fusion zone of welds or laser-remelted specimens. As an example, Figure 5 shows the grain structure seen in the top section of an AISI type 409 stainless steel specimen which has been welded with a gas-tungsten arc (GTA).[26] As can be seen, the grains mainly form by epitaxial growth from the partially remelted grains located at the periphery of the fusion zone. A mechanism of grain competition eliminates the poorly oriented grains. The welding speed (3 mm/s) and the low thermal conductivity of stainless steel produce a rather elongated melt pool. As a result, the grains grow almost perpendicular to the weld direction and the weld centerline is clearly delineated.

III. CAFE MODEL

The cellular automaton algorithm and its integration within FE heat flux computations have been described in detail in Reference 22; therefore, only the basic principles will be summarized here. This model is schematically illustrated in Figure 6.

The physical phenomena which are illustrated in the upper part of this figure are as follows. The extension of a grain in an open region of liquid is first reproduced on the left of this figure with the growth of secondary and tertiary branches, similarly to what has been already described in Figure 3. Assuming flat isotherms, these arms are more undercooled than the stationary primary dendrite tips and accordingly grow faster. Competition among columnar grains is also illustrated for three grains in this figure. The two columnar grains on the right and left of this figure are assumed to be perfectly oriented in the heat flow direction (*i.e.*, vertical ⟨100⟩ trunk direction), whereas the dendrites belonging to the central grain have their ⟨100⟩ trunk direction misoriented by an angle, θ, with respect to the thermal gradient. In order to follow the velocity, v_L, of the liquidus isotherm, T_L, the dendrites of this latter grain have to grow with a higher velocity, v_θ, and thus their undercooling, $\Delta T(v_\theta)$, is larger than in the case $\theta = 0$ deg ($\Delta T(v_\theta) > \Delta T(v_0)$). In a constant thermal gradient, G, their tips lie slightly behind those of the well-aligned neighbor grains (*i.e.*, $\Delta z_\theta > \Delta z_0$, where Δz is the distance between the liquidus isotherm and the primary dendrite tips). Two distinct grain competition situations are then encountered. For the two grains on the left, the ⟨100⟩ directions are converging and the grain boundary is locked to the direction of the best aligned dendrites (*i.e.*, left grain). For the two grains on the right, the dendrite trunk directions are diverging and an open region of liquid continuously forms during solidification. Secondary branches can grow in this region from both side dendrites, and the grain boundary is finally at some intermediate angle between 0 and θ. Since the central grain cannot expand to the left and is gradually overgrown from the right grain, it is expected to disappear over some distance. Such a finding has been discovered indeed during the growth of organic alloys[27] and has been reproduced by the CAFE model described subsequently.[22] Finally, within the undercooled region ahead of the columnar grains, equiaxed grains can form by heterogeneous nucleation and may eventually block columnar grains if they have enough time to grow. This phenomenon should also be reproduced by the CAFE model.

The basic principle of the CAFE model is described in the bottom portion of Figure 6. The simulation domain is first divided into a certain number, N_e, of elements (triangles in the case illustrated here) as for any FE calculation. These elements are used for the heat flow computations: the temperature, T_i and enthalpy, H_i, are defined at each node, i, of this enmeshment.* The software *3-MOS*[23] has been chosen as the host software for that purpose. It keeps the volumetric enthalpy as the free variable (enthalpy formulation) and uses an implicit time-stepping scheme, *i.e.*, the temperatures appearing in the diffusion term of the heat flow equation are taken at the next time-step. The variation of enthalpies at the FE nodes, δH_i, during one time-step can thus be found. For all the nodes which do not belong to the solidifying medium (*e.g.*, the mold), the conversion of δH_i into a variation of temperature, δT_i, is straightforward using a unique temperature-enthalpy relationship. For the nodes located within the solidifying alloy, these variations, δH_i, are converted according to the CA algorithm.

Prior to starting the solidification calculation, the volume of the melt is subdivided into N_c regular square cells superimposed to the FE mesh (Figure 6(b)). This CA enmeshment is fully automated in the preprocessor once the FE mesh has been created. The following entities are then defined for each cell ν: (1) the index of the element to which the cell belongs; (2) coefficients which allow interpolation of any field from the FE nodes to the CA cells; (3) a "boundary reference" index equal to zero if the cell belongs to the bulk of the melt and equal to the reference number of the corresponding boundary if it is at the surface of the domain; and (4) a "crystallographic" index, Ic_ν, which is initially set to zero meaning that the cell is liquid. During solidification, this index can become a positive in-

*Uppercase, lowercase, and greek letters are used for the indices of the FE elements, FE nodes, and cells, respectively.

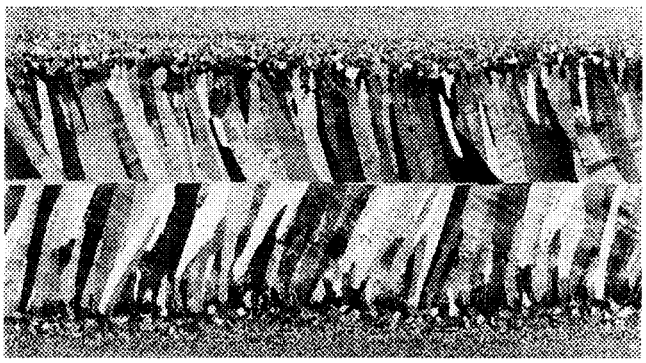

Fig. 5—Grain structure at the top surface of a GTA weld in a stainless steel plate.[26] Remelted width: 9 mm.

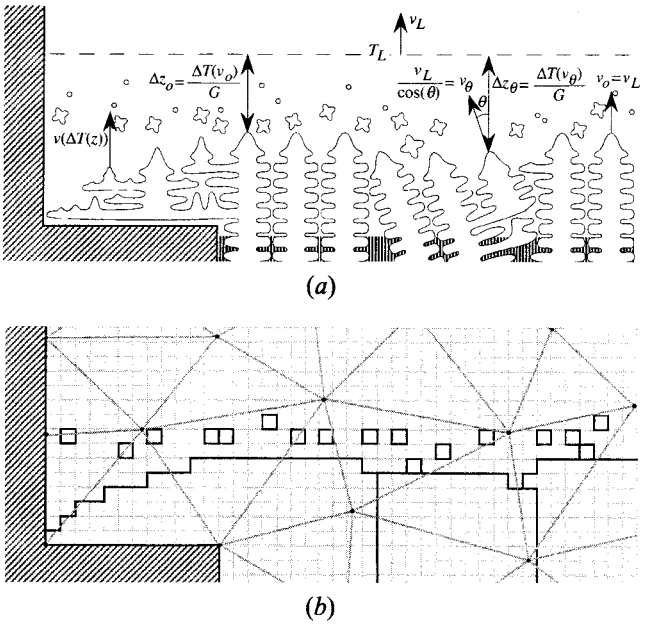

Fig. 6—Schematic diagrams showing (*a*) the mechanisms of dendrite growth and (*b*) the FE mesh and CA grid. The grain boundaries and grain envelopes corresponding to situation (a) are outlined with heavy lines in (b).

teger ($1 \leq Ic_\nu \leq 45$), each value corresponding to a given misorientation of the dendritic network within the cell with respect to the axes of the CA network. The transition of Ic_ν, which is the core of the CA algorithm, can occur according to nucleation and dendrite growth mechanisms, as described subsequently.

For the nucleation in the bulk of the specimen, a certain number of "nucleation cells" are randomly selected prior to starting the solidification calculation. The number of these cells and their critical nucleation undercooling, ΔT_ν^{nuc}, are chosen according to a predetermined nucleation distribution (*e.g.*, a Gaussian law).[8] A similar procedure is applied to the cells belonging to the various boundaries of the domain with appropriate nucleation distributions. If, at a given time, the local temperature, T^t_ν, of a nucleation cell which is still liquid becomes smaller than the prescribed nucleation temperature ($T_L - \Delta T_\nu^{nuc}$), then a new grain forms. The index number of this cell, Ic_ν, is then randomly selected among the 45 predetermined orientation classes.

The dendritic network initiated from a nucleation cell has $\langle 100 \rangle$ directions given by the corresponding orientation class. The envelope of this dendritic network is assimilated locally to a square whose $\langle 100 \rangle$ diagonals grow with the velocity of the dendrite tips. This velocity, v, is a function of the local undercooling, ΔT_ν, of the cell, ν, *via* the growth kinetics model of Kurz *et al.*[28] At a certain time, this dendritic network reaches the position of the four neighbor cells, μ; the growth procedure for the central cell is then ended and restarted from these neighbors using their corresponding undercooling. The crystallographic index number is, of course, transmitted through this growth process (*i.e.*, $Ic_\mu = Ic_\nu$). This simple CA growth algorithm, which allows propagation of the dendritic network from cell to cell, has a major drawback: it biases the original misorientation of the grain to the directions of the CA axes.[18] Refined algorithms have been developed which eliminate this problem.[18,22] Since the extension of the dendritic network associated with each nucleus is simulated by the extension of the grain envelope, the competition of the grains and thus their boundaries are a direct output of the CAFE model (bold lines in Figure 6(b)).

Knowing how to propagate the dendritic network using the CA algorithm, the variation of the volume fraction of solid of each cell, $\delta f_{s,\nu}$, can be easily calculated at each time-step according to the following cases:

(a) The cell ν is liquid at time t and is not captured by a growing grain during δt. Then, $\delta f_{s,\nu} = 0$.
(b) The cell ν is a nucleation cell and is still liquid at time t. If $T^t_\nu \leq T_L - \Delta T_\nu^{nuc}$, then the cell nucleates and $\delta f_{s,\nu} = F_s(T_L - \Delta T_\nu^{nuc})$, where $F_s(T)$ is the function giving the internal volume fraction of solid of the cell according to Scheil.[2]
(c) A liquid cell ν is captured by a growing grain at the temperature T^t_ν, in which case, $\delta f_{s,\nu} = F_s(T^t_\nu)$.
(d) The cell is mushy ($0 < f_{s,\nu} < 1$) in which case the evolution of the volume fraction of solid is calculated according to Scheil.
(e) The cell is already fully solid and thus $\delta f_{s,\nu} = 0$.

Once the variations of the volume fraction of solid, $\delta f_{s,\nu}$, of all the cells have been calculated with the CA, their values are summed up in order to calculate the variation of the volume fraction of solid, $\delta f_{s,i}$, at the node locations. The new temperatures $T_i^{t+\delta t}$ are then deduced according to the heat balance $\delta H_i = c_p \cdot \delta T_i - L \cdot \delta f_{s,i}$, where c_p and L are the volumetric specific heat and latent heat, respectively.

The model described in Reference 22 corresponds to a *full coupling* between the FE and CA models: at each time-step, the variations of enthalpy at the FE nodes are converted into specific and latent heat contributions using the CA algorithm. It was shown that recalescences can be calculated in this way. If the thermal gradient within the specimen is large, a *semicoupling* can be used: the temperature field is calculated first for all the time-steps, using a Scheil microsegregation model; then, at each time-step, the CA is applied as a module for the nucleation and growth of the grains only (*i.e.*, the latent heat released by the cells is no longer calculated in the procedure described in points (a) through (e) but is deduced from a unique temperature-enthalpy relationship). Finally, the time-step at the CA level must be such that the extent of the dendritic network during δt is smaller than the size of the cell (*i.e.*, propagation from neighbor to neighbor).

IV. RESULTS AND DISCUSSION

A. *Investment Cast Turbine Blades*

The first application is related to the investment casting of a turbine blade. Since the CAFE model is still 2-D, Figure 7(a) must be viewed as a 2-D longitudinal section of a blade. The grain selector has been highly idealized as a simple zigzag and an extra reservoir of molten metal at the top of the blade has been designed (heat reservoir). This figure shows the 2-D enmeshment used for the heat flow computations; it is made out of 2295 elements and 1739 nodes. As can be seen, both triangles and quadrangles can be used. The enlargement view located on the left of Figure 7(a) corresponds to the left corner of the bottom platform. This zoom shows both the FE and CA enmeshments, the latter consisting of 68,386 square cells defined for the metal part only. The inclined boundaries of the solidifying domain are approximated by steps, as with the FD method.

The final structure of the grains calculated for this blade with the fully coupled CAFE model is shown in Figure 7(b), the gray color of the grains corresponding to their crystallographic orientation. The growth kinetics of the multicomponent CMSX6 alloy was calculated as indicated in References 19 and 29. As demonstrated in Reference 22 for one-dimensional aluminum castings, nucleation parameters can be deduced from the measured undercoolings and final grain morphologies. In the present case, a set of nucleation parameters was chosen for the bulk of the liquid, for the bottom boundary in contact with the copper chill, and for the lateral surface of the blade in contact with the ceramic mold so as to reproduce qualitatively the final grain structure shown in Figure 2(a). The thermal parameters were taken from the work of Imwinkelried.[29] The various steps of the solidification process are shown in Figures 7(c) through (i).

Figures 7(c) and (d) show the temperature distribution and the grain structure, respectively, in the bottom part of the grain selector at time $t = 30$ seconds. The temperature scale (1012 °C to 1312 °C) was chosen so as to reveal the position of the liquidus front ($T_L = 1312$ °C) and to give

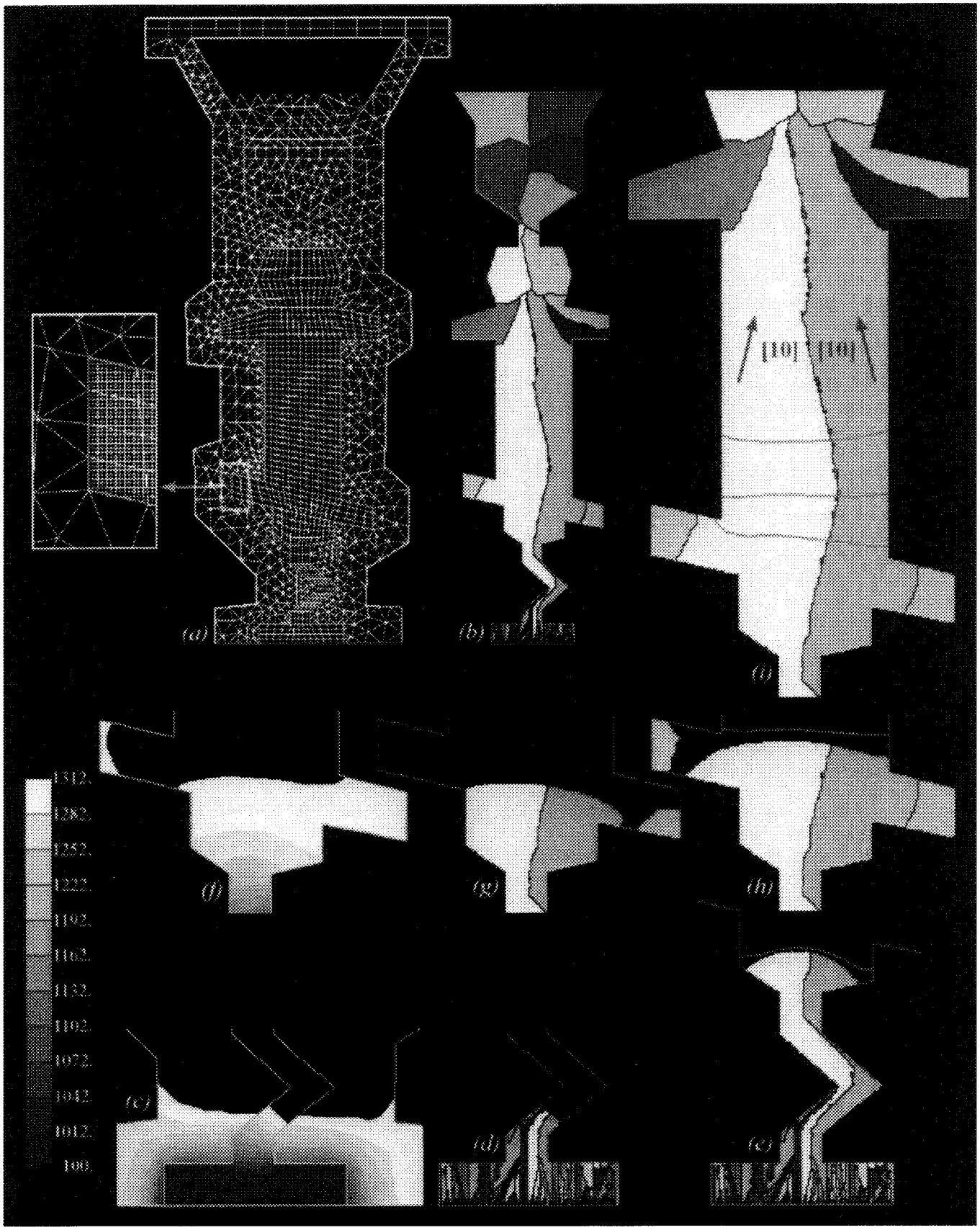

Fig. 7—(*a*) Enmeshment and (*b*) final grain structure in a 2-D turbine blade. (*c*) through (*i*) The various stages of solidification (see text).

an indication of the thermal gradient. Therefore, all the liquid metal above T_L is dark. From the shape of the liquidus line, it can be seen that the heat flux is essentially following the zigzag of the grain selector in contact with the copper chill. (The contact between the casting and the chill is modeled *via* a heat-transfer coefficient). This is expected since the mold was preheated to the temperature of the metal and there was not much lateral radiation loss (*i.e.*, almost adiabatic ceramic mold at short time). As can be seen in Figure 7(d), many grains are nucleated at the surface of the chill plate with a random crystallographic orientation. As growth proceeds, the grains whose ⟨100⟩ crystallographic directions are poorly aligned with the almost vertical heat flux are eliminated and only a few grains enter the selector. These grains have to turn in order to follow the change in the orientation of the thermal gradient and their selection is modified accordingly. (It should be pointed out that only the boundaries of the grains turn; their crystallographic orientation remains the same).

After the first turn of the selector (Figure 7(e)), only the two grains seen in the final airfoil remain. They emerge then in the larger section of the blade above the selector (t = 230 seconds). Since most of the heat flux still goes through the grain selector, the isotherms are curved and the resulting interface of the two grains is convex in Figure 7(e). The line above the two grains corresponds to the actual position of the liquidus isotherm, thus outlining the undercooled liquid region. At time t = 320 seconds, the liquidus temperature is already above the first platform on the right of the blade, as indicated by the temperature map shown in Figure 7(f) (same temperature scale as before). However, due to lateral radiation, the left corner of the platform is also cooled down below T_L. Since the dendritic network has to propagate in these open regions of liquid, the grain structure has the morphology shown in Figure 7(g). At the right corner of the platform, the right-hand-side grain starts to extend in a way similar to that shown in Figure 3. Since the ⟨100⟩ directions of the branches are not parallel to the bottom surface of the platform, tertiary arms have to propagate downward, as in Figure 3, thus resulting in a small cusp in the envelope of the dendritic network. Before this grain can reach the end of the platform, a new grain has nucleated at the right corner. At time t = 400 seconds (Figure 7(h)), the right part of the platform is already filled by dendrites but the left one is not yet fully mushy, even though the liquidus isotherm (line drawn in the liquid above the interface of the two grains) is almost flat and located above the platform within the airfoil. As can be seen, another stray crystal has also formed in this part of the platform.

Figure 7(i) is an enlargement of the final grain structure calculated for the airfoil. The ⟨100⟩ crystallographic orientations of the two crystals are indicated by arrows: the left-hand-side grain has a misorientation of −14 deg with respect to the axis of the blade, whereas the right-hand-side grain is misoriented by +14 deg. The three lines superimposed on this figure correspond to the position of the liquidus isotherm at t = 360, 440, and 520 seconds. As can be seen, the liquidus front which is slightly convex at the exit of the first platform becomes flat and then concave as solidification proceeds. This change in the thermal gradient has a direct influence on the shape of the grain boundary. Since the two grains have converging ⟨100⟩ orientations, the grain boundary must be aligned with the direction of the dendrites which are best aligned with the heat flux.[22] Therefore, at the bottom of the airfoil, the growth of the left grain is favored because the thermal gradient is slightly oriented toward the right and the resulting grain boundary is parallel to the ⟨100⟩ direction of this grain. When the liquidus isotherm becomes concave, the situation is reversed: the thermal gradient points toward the left and the right grain dominates the left one.

Since both the grain structure and the temperature field can be visualized in *3-MOS*, the shape of the grain boundary can be explained quite easily using the CAFE model. This shape results from the interplay between the orientation of the heat flux (or thermal gradient) and the mutual crystallographic misorientations of the grains. The situation of diverging crystallographic orientations could have been analyzed as well.

The fact that the grains coming out of the grain selector are not precisely oriented along the heat flux direction has already been explained using the 3-D stochastic model:[21] the probability, $dp/d\theta$, of finding a grain with its ⟨100⟩ direction aligned at an angle θ with the thermal gradient is proportional to $\sin(\theta)$ and thus tends toward zero as $\theta \rightarrow 0$. In the present 2-D situation, however, $dp/d\theta$ is uniform between −45 and +45 deg. Therefore, the orientation distribution of the grains should narrow symmetrically around $\theta = 0$ deg as the selection mechanism operates within the columnar zone. At the height of the first right turn of the grain selector, the orientation distribution is not yet very narrow since this selection has occurred over a short distance only. Subsequently, the shape of the zigzag eliminates some of the remaining grains, mainly by geometrical obstruction. Simultaneously, the thermal gradient direction changes as heat is flowing by conduction through the grain selector (Figure 7(c)). However, these two phenomena do not choose grains which are best oriented along the axis of the blade. In summary, the orientation of the grains within the airfoil mainly results from the grain competition occurring below the first turn of the selector.

B. *Continuously Cast Rods*

The effects of inoculation and withdrawal speed on the temperature field and grain structure of continuously cast rods are shown in Fig. 8. In this case, 20-mm-diameter Al-Si rods were continuously cast at two casting speeds: (a) 1 mm/s and (b) 5 mm/s. The corresponding stationary thermal fields shown at the center of the figure (a1 and b1) were first calculated using the macroscopic FE model only; *i.e.*, the new temperature at each FE node was directly deduced from the corresponding variation of enthalpy using the Scheil approximation. The CA model was then used as a postprocessor module for the prediction of the grain structure in each case. Such a semicoupled FE-CA approach is, of course, much simpler to implement than the fully coupled scheme presented earlier but is perfectly valid as long as the thermal gradient is large. It also allows the use of a Eulerian representation for the calculation of the stationary thermal field (*i.e.*, the reference frame is attached to the mold, and the transport term $v \cdot \text{grad}(H)$, where v is the casting speed, appears in the heat flow equation for the rod), whereas the CA calculation is based upon a Lagrangian

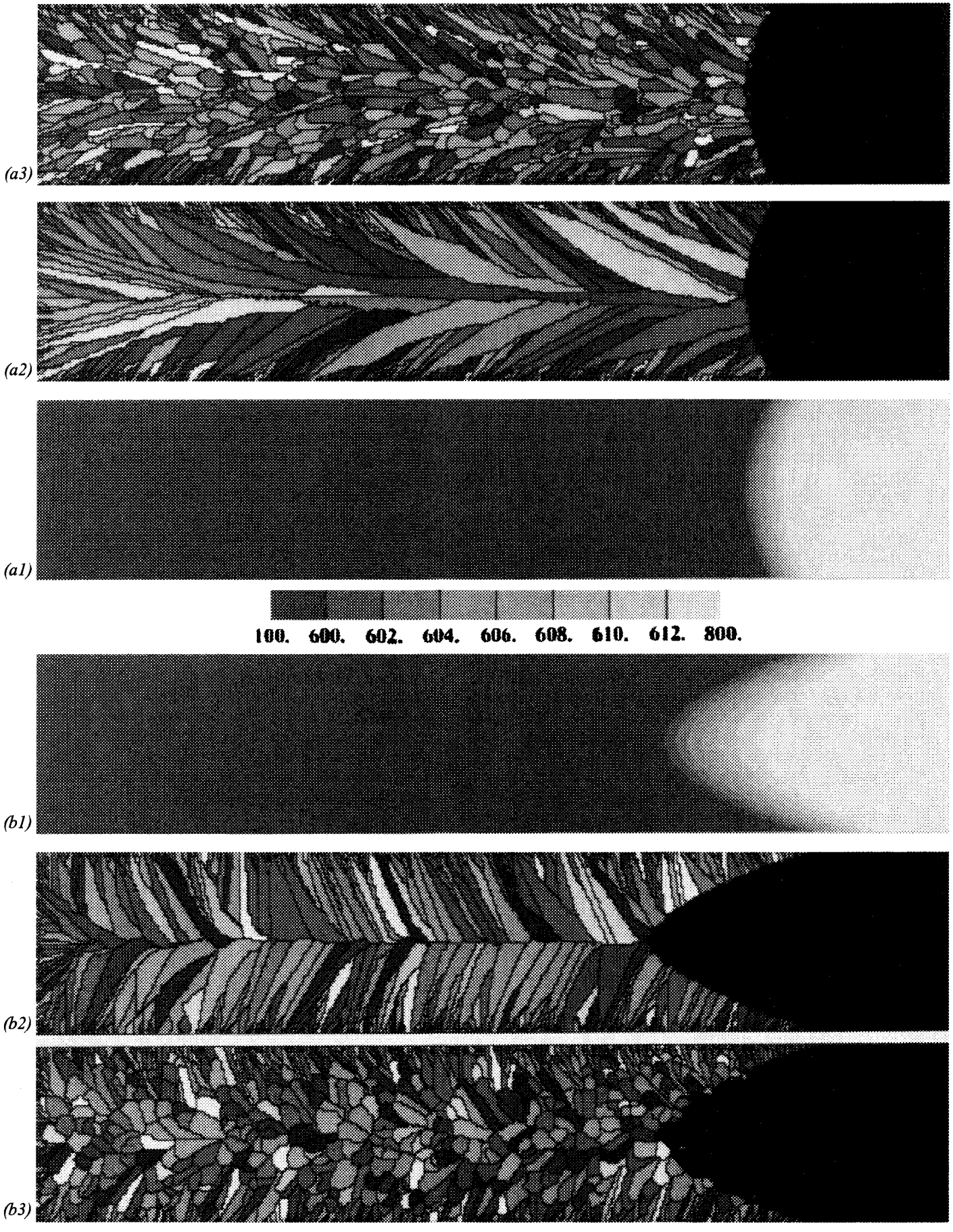

Fig. 8—Grain structures and temperature maps within the longitudinal section of two rods produced by continuous casting at two withdrawal speeds: (*a*) $v = 1$ mm/s and (*b*) $v = 5$ mm/s.

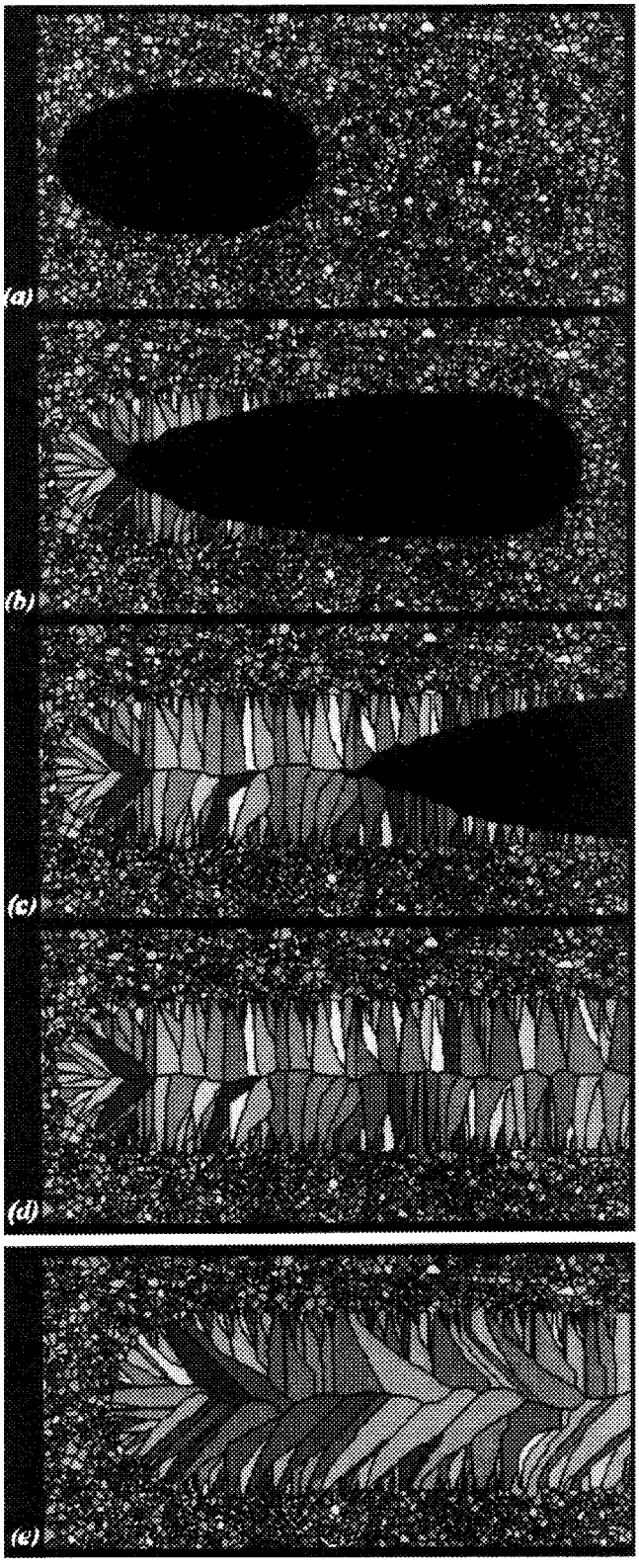

Fig. 9—Grain structures at the top surface of a specimen remelted by a moving heat source: (*a*) initial equiaxed structure and shape of the "equilibrium" molten pool; (*b*) through (*d*) formation of the grains in the fusion zone; and (*e*) the final grain structure obtained with a velocity 5 times lower than that in (d).

description (*i.e.*, the cells are attached to the moving rod). A Lagrangian representation could have been used for both the FE and CA calculations, in which case, the cooling conditions associated with the mold would have been translated along the lateral surface of the nonmoving rod.

As can be seen in Figure 8, the isothermal lines are almost flat at 1 mm/s (a1), whereas the sump depth is nearly equal to the radius of the rod at 5 mm/s (b1). The temperature scale is shown in between the two cases. Assuming that nucleation could only occur at the surface of the rod, the two columnar structures of Figure 8 are obtained (a2 and b2). The undercooling of the columnar dendrite front can be directly estimated with the help of the thermal maps; it is, of course, larger for the higher casting speed. In order to follow the nearly flat isotherms of the low-speed conditions, the grains progressively turn as they grow (macroscopically not crystallographically), thus reproducing qualitatively the experimental observations shown in Figure 4. Because of their shape, the grains do not meet precisely at the rod centerline and are interlaced. In contrast, the columnar structure calculated for the high casting speed is nearly perpendicular to the side of the rod due to the much deeper sump profile, and the grains meet precisely at the centerline. The segregation associated with the formation of such a centerline is incompatible with the subsequent extrusion of these rods. This obviously limits the casting speed of alloys for which inoculation of the liquid bulk cannot be enhanced (*e.g.*, copper-base alloys).

For most aluminum alloys, titanium diboride is used as a grain refiner. The effect of a grain refiner is shown in Figure 8 for the two rods cast under identical thermal conditions (a3 and b3). Some of the grains which form in the undercooled liquid can be seen as isolated dots in the black regions. They are more visible at high casting speed for which the undercooling is maximum. These grains then grow in a thermal gradient, G, which decreases from the lateral surface to the center of each rod. Please note also that the gradient at the center of the rod is parallel to the axis of symmetry and is lower at higher casting speed (bottom). This situation is essentially the same as that previously reported for eutectic grains growing in a thermal gradient:[17] the grains nucleating in the bulk of the liquid are elongated in the upstream heat flux direction as a result of their impingement and their elongation is an increasing function of $(G \cdot v_s^{-1})$, where v_s is the local solidification rate.* Accordingly, the grains are more elongated at low casting speed (Figure 8, a3) and at the periphery of the rods. Nearly equiaxed grains are seen in the center of the inoculated rod cast at 5 mm/s (Figure 8, b3) for which the casting speed is maximum and the gradient is minimum.

*In a stationary situation, $v_s = v \cdot \cos(\theta)$, where θ is the angle between the axis of the rod and the thermal gradient.

C. *Laser Remelting/Welding*

The situation of laser remelting or welding is very similar to continuous casting, except for the nucleation conditions. Indeed, the back of the molten pool (solidification part) in welding is characterized by a thermal field which has the same shape as the one shown in Figure 8. However, the grains in the fusion zone of the weld can now epitaxially grow from the grains which have been partially melted by the upper part of the pool.

This situation is illustrated in Figure 9 for a steel plate remelted by a moving laser. A uniform equiaxed grain

structure was first produced using the CAFE model. It was then remelted using the stationary temperature field solution associated with a moving heat source. Since the Eulerian–Lagrangian representation issue is the same as that encountered in continuous casting, the analytical Rosenthal solution of a point heat source[30] was used here to calculate the temperature at each cell location. It is clear that the stationary temperature solution coming from *3-MOS* could have been used as well. The shape of the molten pool corresponding to the equilibrium liquidus isotherm is shown in Figure 9(a) (black area). As the molten pool is moved toward the right (Figures 9(b) and (c)), grains start to grow in the fusion zone from the partially remelted grains at the periphery. The growth speed of these grains is zero at the maximum width of the fusion zone (transition from melting to solidification) and increases as $v \cdot \cos(\theta)$ as the grains move toward the centerline (θ is again the angle between the moving speed of the heat source and the thermal gradient). Accordingly, the undercooling also increases, and as a result, the actual pool shape is no longer that of an ellipse (imposed by the symmetry of the thermal field) but rather that of a teardrop (Figures 9(b) and (c)). Even though the present CAFE model does not consider the overlap of the solute layers at the impingement of the dendritic grains growing from both sides of the melt pool, it is able to predict the teardrop shape of the molten pool actually seen in experiments at high welding speed,[31] whereas a pure thermal calculation fails to explain such a shape. Please note that the final grain structure in the fusion zone (Figure 9(d)) is very close to the experimental micrograph shown in Figure 5. When the travel speed of the moving heat source is lowered (Figure 9(e)), the undercooling of the dendrites becomes lower at the same time the pool becomes more hemispherical and the grains have a tendency to align along the welding direction.

V. CONCLUSIONS

Although the CAFE model presented here is still 2-D, it brings a valuable insight into the mechanisms of grain structure formation in various solidification processes. Several examples have been shown which illustrate qualitatively how the grain structure of an alloy is related to the casting and inoculation conditions. The grain selection mechanisms in the columnar zone of DS turbine blades, the transition from columnar-to-equiaxed structures, the formation of stray crystals at section changes of the mold, and the influence of the thermal gradient direction on the shape of the grain boundaries have been demonstrated for an investment cast turbine blade. Two other applications related to continuous casting and welding have also been shown.

At present, the 2-D CAFE model implemented in *3-MOS* is a very good learning and teaching tool, because it allows direct viewing of the formation of the grains as solidification proceeds. In its present form, it can be employed to study the formation of grains in some critical 2-D sections of castings, using the thermal information obtained from a 3-D heat flow calculation. The CET and the formation of stray crystals are two mechanisms which can be studied with the present 2-D CAFE model. It also allows one to have access to the nucleation parameters *a posteriori* if the other parameters (growth kinetics and casting conditions) are known.

There is no extra work involved in the definition of the CA mesh from the FE enmeshment and the extra CPU time is rather limited, especially when using the CA as a post-processor module. The calculation shown in Figure 7 (2'295 elements, 68'386 cells, and 15'490 time-steps) runs in less than 3 hours on a HP755* workstation. This computation time could be considerably reduced if the fine time-step dictated by the CA algorithm was decoupled from the time-step used in the implicit heat flow computations (*i.e.*, two time-steps algorithm[23]). Unlike implicit FE calculations, the CPU time associated with the CA part is a linear function of the number of cells and can be highly optimized. Furthermore, the CA calculation needs to be done only for those cells located within the elements which are undercooled and still contain liquid cells. Therefore, it is realistic to envisage to extend the present CAFE model to three dimensions. Such an extension has been done under the limitation of uniform temperature situations[19,20,21] and has already brought quantitative answers regarding the evolution of the grain density and texture. The full 3-D CAFE model should be an important simulation tool for the investment casting industry (*e.g.*, optimization of the grain selector shape, of the casting conditions, and of the yield rate) as well as for other solidification processes for which the grain structure is important.

*HP755 is a trademark of Hewlett-Packard Company, Colorado Springs, CO.

ACKNOWLEDGMENTS

The authors would like to thank the Commission pour l'Encouragement de la Recherche Scientifique, Berne, for its financial support under Grant No. 2361.1. The companies Sulzer Innotec, Winterthur (CH), and Swissmetal Boillat, Reconvilier (CH), as well as Professor H.W. Kerr are gratefully acknowledged for making available the specimens shown in Section II.

REFERENCES

1. B. Chalmers: *Principles of Solidification*, John Wiley and Sons, New York, NY, 1964.
2. W. Kurz and D.J. Fisher: *Fundamentals of Solidification*, Trans Tech Publications, Aedermannsdorf, Switzerland, 1989.
3. M. McLean: *Directionally Solidified Materials for High Temperature Service*, The Metals Society, London, 1983.
4. S.C. Huang and M.E. Glicksman: *Acta Metall.*, 1981, vol. 29, pp. 701-15 and 717-34.
5. K. Somboonsuk, J.T. Mason, and R. Trivedi: *Metall. Trans.*, 1984, vol. 15A, pp. 967-75.
6. H. Esaka and W. Kurz: *J. Cryst. Growth*, 1985, vol. 72, pp. 578-84.
7. F. Staub, B. Walser, and J. Wortmann: *Rev. Tech. Sulzer*, 1988, vol. 3, pp. 11-16.
8. M. Rappaz: *Int. Mater. Rev.* 1989, vol. 34, pp. 93-123.
9. S.G.R. Brown and J.A. Spittle: *Mater. Sci. Technol.*, 1989, vol. 5, pp. 362-68.
10. J.A. Spittle and S.G.R. Brown: *Acta. Metall.*, 1989, vol. 37, pp. 1803-10.
11. M.P. Anderson, D.J. Srolovitz, G.S. Grest, and P.S. Sahni: *Acta Metall.*, 1984, vol. 32, pp. 783-91.

12. P. Zhu and W. Smith: *Acta Metall.*, 1992, vol. 40, pp. 683-92.
13. P. Zhu and W. Smith: *Acta Metall.*, 1992, vol. 40, pp. 3369-79.
14. M. Rappaz and Ch.-A. Gandin: *MRS Bull.*, 1994, vol. XIX, pp. 20-24.
15. Ch. Charbon and M. Rappaz: *Model. Simul. Mater. Sci. Eng.*, 1993, vol. 1, pp. 455-66.
16. Ch. Charbon, A. Jacot, and M. Rappaz: *Acta Metall.*, 1994, vol. 42, pp. 3953-66.
17. M. Rappaz, Ch. Charbon, and R. Sasikumar: *Acta Metall.*, 1994, vol. 42, pp. 2365-74.
18. M. Rappaz and Ch.-A. Gandin: *Acta Metall.*, 1993, vol. 41, pp. 345-60.
19. Ch.-A. Gandin, M. Rappaz, and R. Tintillier: *Metall. Trans. A*, 1993, vol. 24A, pp. 467-79.
20. Ch.-A. Gandin, M. Rappaz, and R. Tintillier: *Metall. Trans. A*, 1994, vol. 25A, pp. 629-35.
21. Ch.-A. Gandin, M. Rappaz, D. West, and B.L. Adams: *Metall. Trans. A*, 1995, vol. 26A, pp. 1543-51.
22. Ch.-A. Gandin and M. Rappaz: *Acta Metall.*, 1994, vol. 42, pp. 2233-46.
23. Ph. Thévoz, M. Rappaz, and J.-L. Desbiolles: in *Light Metals*, Ch.M. Bickert, ed., TMS, Warrendale, PA, 1990, pp. 975-84.
24. W.B. Dress, T. Zacharia, and B. Radhakrishnan: Conference proceeding, *Modeling and Control of Joining Processes*, Ed. T. Zacharia, AWS/ORNL, 1993, pp. 321-28.
25. Ch.-A. Gandin: Ph.D. Thesis, Ecole Polytechnique Fédérale de Lausanne, Lausanne, Switzerland, 1994.
26. J.C. Villafuerte, E. Pardo, and H.W. Kerr: *Metall. Trans. A*, 1990, vol. 21A, pp. 2009-19.
27. H. Esaka, J. Stramke, and W. Kurz: *Columnar Dendrite Growth in Succinonitrile-Acetone Alloys*, Film, Ecole Polytechnique Fédérale de Lausanne, Lausanne, Switzerland, 1985.
28. W. Kurz, B. Giovanola, and R. Trivedi: *Acta Metall.*, 1986, vol. 34, pp. 823-30.
29. Th. Imwinkelried: Ph.D. Thesis, Ecole Polytechnique Fédérale de Lausanne, Lausanne, Switzerland, 1993.
30. J.F. Lancaster: *Metallurgy of Welding*, 3rd ed., G. Allen and Unwin Publishing, London, 1980.
31. K. Easterling: *Introduction to the Physical Metallurgy of Welding*, Butterworth and Co., London, 1983.